BINDER SYSTEM EFFECT ON THE MICROSTRUCTURE AND PROPERTIES OF INSULATING CERAMIC FOAMS

Tiago dos Santos Jr[1], Gustavo Cogo e Silva[1], Vânia Regina Salvini[1], Victor Carlos Pandolfelli[1]

[1]Universidade Federal de São Carlos, São Carlos, Brazil

ABSTRACT

Energy saving methods arise from two main routes: efficiency and conservation. The former reduces the energy required to perform a task, whereas the latter comprises all actions to reduce the losses. For high temperature processes, heat conduction is mostly carried out by radiation in the infrared range (0.7 to 100 µm). Therefore, a good thermal insulating material for high temperature application must be able to reduce the radiation intensity within the temperature of interest. Porous refractory ceramics with tailored amount and size of pores are candidates to be applied for this purpose. Considering the different routes of processing porous ceramics, the direct foaming method results in materials with reproducible properties, narrow distribution of pore sizes and suitable mechanical strength. Nevertheless, physical effects as coalescence and drainage can take place in the liquid foam, reducing its stability and increasing the bubbles' size. There are two ways to control this phenomena: adding surfactants that act on the bubble's surface tension or using binders that induce the fast transition from the liquid to solid foam. In this work, aluminous foams were prepared by the direct foaming method using different inorganic binder systems and setting additives. Their microstructure, porosity, thermal conductivity and mechanical strength, were evaluated. The results pointed out that the foam microstructure was modified when different binder systems were used, influencing the mechanical and thermal properties of the material. Based on these results, the selection of the binder system has been shown an important factor to process porous material with tailored properties.

INTRODUCTION

Energy saving methods arise from two main routes: efficiency and conservation. The efficient use of energy is achieved when systems are designed to work in a rational way, demanding the lowest level of power as possible. On the other hand, conservation comprises all actions to reduce the energy losses. For high-temperature processes, heat is the main source of energy. It can be transported by conduction via phonons or electrons through the solid media; by the convection of fluids or by the radiation emitted by the materials [1]. The microstructure of porous insulating refractories is designed to minimise these transport phenomena by adjusting the amount, the morphology, the size of the pores and the mineralogical composition. For instance, the presence of calcium hexaluminate (CA_6) in an aluminous foam could improve the thermal insulation properties of this material [1].

At temperatures higher than 1000°C, the radiation becomes an important mechanism for heat transportation, where infrared radiation is emitted and can propagate, carrying energy. The photons can be absorbed by the solid phases or scattered by structures with sizes close to the radiation's wavelength [1]. Hence, the share of radiation to the heat transport can be reduced by a microstructure comprising pores with specific sizes and closed walls.

Among the different routes of processing porous ceramics, the direct foaming methods comprehends the techniques in which a gas is incorporated into a ceramic suspension [2]. As bubbles are created, the liquid-gas interfaces need to be stabilised by additives such as small amphiphilic molecules, protein micelles or solid particles [3]. After the gas incorporation and stabilisation, a liquid foam is obtained, and its solidification results in a solid material with high porosity [4].

As the liquid foam is thermodynamically unstable, drainage, coarsening and coalescence take place in order to change it. These physical effects should be minimised to preserve the foam microstructure. One possible route to avoid the growth of the bubbles could be the kinetic control of the solidification. In this context, the transition from a liquid ceramic foam to a solid could be directed by the binder system. Taking calcium aluminate cement (CAC) for instance, it could be possible to adjust its hydration kinetic in order to speed up the solidification and prevent the foam destabilisation. Lithium sources could be used to speed up the CAC hydration, as the association of Li^+ with aluminium ions generates lithium aluminates. These compounds act as heterogeneous nuclei for growing calcium aluminate hydrates [5]. On the other hand, the dispersion of CAC particles prior to their addition to the aqueous foam could also help to accelerating the solidification, as more active surfaces would be exposed to the aqueous media. Nevertheless, due to the high reactivity of CAC particles in water, their dispersion should be carried out only at the moment of adding it to the alumina foam.

In this work, the effects of a lithium source and a dispersing agent on the stabilisation of alumina-CAC foams were studied. The compositions were processed by a direct foaming route and their kinetics of solidification, microstructure and mechanical properties, were characterised.

MATERIALS AND METHODS

Three foam compositions were formulated using the Andreassen packing model (q = 0.37, Tab. 1). In order to produce the foams by the direct foaming method, an alumina suspension was initially prepared. Reactive aluminas ($d_{50} \leq 2.5$ µm) were added to the aqueous solution containing the polyethylene glycol based dispersing agent (PEG). The suspension was kept under shearing and an ethoxylated alcohol based surfactant (EAS) was added to adjust the wettability of alumina particles. The liquid foam was prepared in another recipient. Initially, an aqueous solution of alpha olefin sulfonate-based surfactant (AOS) was stirred up to the stabilisation of the foam volume. At this point, the hydroxypropyl methyl cellulose (HPMC) was dispersed in the system to increase its stability. The foam was carefully dispersed in the alumina suspension under mild agitation. In the end, the binder system was added. To the first composition, Alumina-CAC (AC), the cement particles were incorporated directly into the alumina liquid foam. For the Alumina-CAC accelerated system (ACA), the cement was initially dispersed in the foam, followed by the addition of lithium carbonate (Li_2CO_3). Regarding the Alumina-CAC dispersed composition (ACD), an aqueous solution of a sodium polymethacrylate-based dispersing additive (PMA) was prepared, and CAC particles were dispersed in this solution. The final suspension was added to the liquid foam. The samples were moulded and cured for 24h at 50°C with 80% of relative humidity. Following, these samples were dried at 110°C for 24h and fired at 1100°C or 1600°C for 5h.

Tab. 1: Composition of the alumina foams prepared

		AC	ACA	ACD
	Components	**wt %**		
Alumina suspensio	**Al_2O_3**	81.78	81.78	81.78
	PEG	0.09	0.09	0.09
	EAS	0.10	0.10	0.10
	Water	15.79	15.79	13.79
Liquid foam	**AOS**	0.162	0.162	0.162
	HPMC	0.0056	0.0056	0.0056
	Water	2.43	2.43	2.43
Binder system	**CAC**	5.0	5.0	5.0
	PMA	0	0	0.0625
	Li_2CO_3	0	0.005	0
	Water	0	0	2.0

The solidification kinetic of the compositions was assessed by *in situ* ultrasound speed measurements at room temperature. An ultrasonic measuring system IP-8 (Ultratest, Germany) was used, and the changes were recorded during 24h. Its evolution was correlated to the solidification of the foams.

Apparent density, total porosity and closed porosity were estimated for cylindrical samples (40 mm x 40 mm) dried at 110°C for 24h or fired at 1100°C or 1600°C for 5h. The samples were kept immerse in water for 24h and the mass of dried (D), suspended (S) and saturated (W) samples, were measured. The apparent density, the total porosity and the closed porosity were calculated using the equations (1), (2) and (3), respectively, where, ρ_l is the density of the immersion liquid, taken as 1.0 $g.cm^{-3}$, and ρ_{th} is the theoretical density of the solid fraction, considered to be 3.4 $g.cm^{-3}$.

$$\text{Apparent density, } \rho_{ap}\ (g.cm^{-3}) = \rho_l * [D / (D - S)] \quad (1)$$

$$\text{Total porosity, } P_{total}\ (\%) = 100 * [1 - (\rho_{ap} / \rho_{th})] \quad (2)$$

$$\text{Closed porosity } (\%) = P_{total} - 100 * \{[(W - D) / (W - S)]\} \quad (3)$$

The dimensional changes (D_f) of five cylindrical bodies (50 mm x 50 mm) of each composition were measured after thermal treatment at 1100°C or 1600°C. The resulting data was compared with those of the samples dried at 110°C for 24h (D_o), and the linear dimensional change was calculated by equation (4). These values are reported as the percentage of shrinkage.

$$\text{Linear dimensional change } (\%) = 100 * (D_f / D_o) \quad (4)$$

The cold crushing strength of cylindrical samples (50 mm x 50 mm) after drying at 110°C for 24h or firing at 1100°C or 1600°C for 5h, was also evaluated. These tests were carried out in an EMIC 23-600 (EMIC, Brazil) following ASTM C133 for insulating refractories [6], with a loading rate of 6.08 $kN.min^{-1}$. The cold crushing strength (CCS) was calculated by equation (5), where F corresponds to the maximum load recorded and A, the samples' loading area.

$$CCS\ (MPa) = F / A \quad (5)$$

The microstructures of samples fired at 1600°C for 5h were observed in a stereo microscope Stemi 2000C coupled with an ERc 5s digital camera (Zeiss, Germany). The microscopic digital images and the software ImageJ were used to measure the pore size distribution of the samples. The reported pore diameters (D_{sph}) were obtained after the stereological correction [7] of the values measured directly from the images, D_{circ}, by equation (6).

$$D_{sph} = D_{circ} / 0.785 \quad (6)$$

RESULTS AND DISCUSSION

The curves of ultrasound speed (US) measured during the foams curing step at room temperature are presented in the Fig. 1. The initial increase in US, observed for the three compositions up to 3h after the beginning of the tests, could be associated with the viscoelastic changes due to the absence of shearing stresses. The main increase, related to the formation of calcium aluminate hydrates, occurred firstly for the composition containing the lithium source. For this system, the onset of solidification was close to 3.5h. The ACD composition had a solidification profile similar to that of AC. For these systems, the US started to increase after 5h of the beginning of the test and pointed out that the dispersion of CAC didn't speed up the hydration.

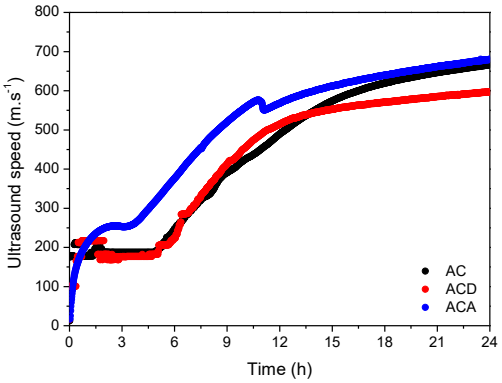

Fig. 1: Ultrasound speed evolution as a function of time at room temperature for the evaluated foams.

The changes in the binder system resulted in variations in the total porosity values, as shown in the Fig. 2(a). Compared to the AC composition, those samples containing lithium carbonate or dispersed CAC presented a reduction in the total porosity, which varied from 74% (AC) down to 70% (ACD).

The closed porosity for ACA and ACD compositions were lower than that for the AC samples [Fig. 2 (b)]. These results indicate that changes in the microstructure were caused by these different binder systems, resulting in variations in the porosity and consequently, in the apparent density. As presented in the Fig. 3, the ρ_{ap} of samples dried at 110°C for 24h increased from AC to ACA and ACD compositions. For the system with the lithium source, the higher amount of calcium aluminate hydrates increased the sample density. The presence of less flocculated CAC particles on the ACD composition also incremented the density of the samples.

Further decomposition of the calcium aluminate hydrates caused the increase in the total porosity of the samples after firing at 1100°C, as shown in Fig. 2(a). This effect resulted in the reduction of the closed pores amount [Fig. 2(b)], followed by a reduction in the apparent density of the samples (Fig. 3). Nevertheless, the formation of CA_2, which is followed by the volumetric expansion [8], and the beginning of the sintering, could take place in this temperature range. These transformations could counteract the creation of pores in the microstructure of the samples.

Sintering and the CA_6 formation were detected during firing the compositions at 1600°C. These samples had an increase of density, followed by the reduction of total and closed porosities. Besides the formation of CA_6, which occurs with a volumetric expansion of up to 3% [8], the samples fired at 1600°C had their dimensions reduced, as the Fig. 4 indicates. The shrinking observed could be associated with the sintering effects which resulted in the densification. Compared to that, the small

dimensional changes detected after 1100°C suggest that effective sintering occurred only at higher temperatures.

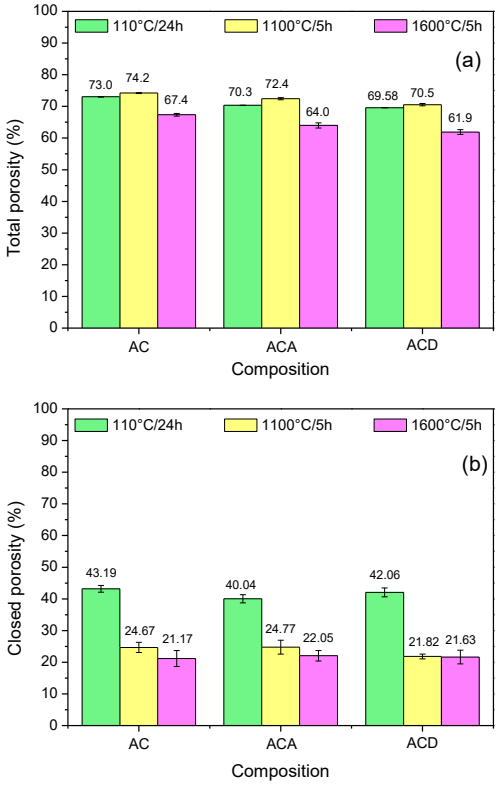

Fig. 2: Total and closed porosities of samples previously dried at 110°C for 24h or fired at 1100°C or 1500°C for 5h.

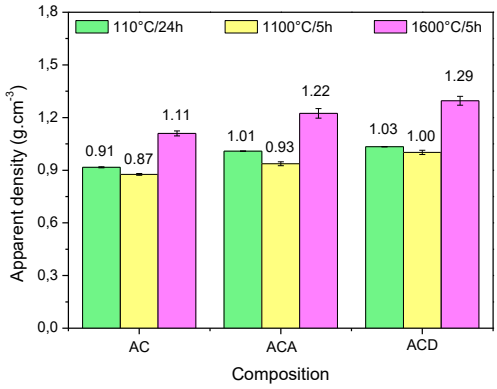

Fig. 3: Apparent density of samples dried at 110°C for 24h or fired at 1100°C or 1600°C for 5h.

The mechanical strength evolution of the compositions is presented in the Fig. 5. For both systems, the cold crushing strength values increased from samples dried at 110°C to those fired at 1100°C. Besides the generation of pores in the compositions fired at 1100°C, the partial sintering could justify the increase of the mechanical strength. Samples fired at 1600°C presented the higher values of cold crushing strength, which increased from AC and ACA to ACD samples, in this order. Alumina-CAC accelerated samples reached a value of mechanical strength 1.6-fold higher than that of the Alumina-CAC whereas ACD samples presented an average value 2.6-fold superior.

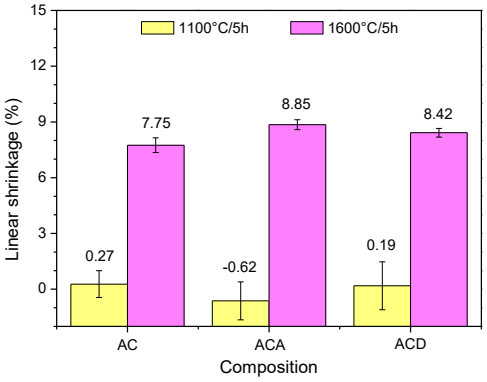

Fig. 4: Dimensional changes registered after firing the samples at 1100°C or 1600°C for 5h. The dimensions of samples dried at 110°C for 24h were taken as references for these measurements.

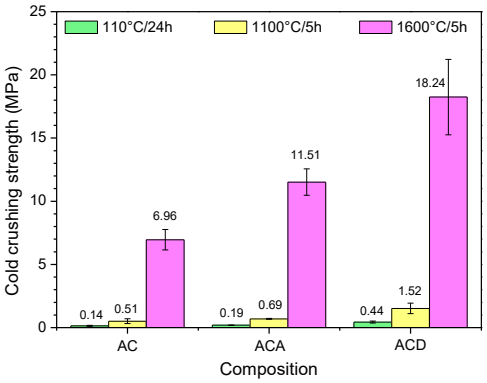

Fig. 5: Mechanical strength evaluated at room temperature for samples dried at 110°C for 24h or fired at 1100°C or 1600°C for 5h.

The effects of the binder systems in the mechanical strength could be related to the generation of homogeneous microstructures. Lithium carbonate could induce the formation of nuclei better scattered in the system [5]. By this mechanism, calcium aluminate hydrates could be formed in the whole microstructure, developing the mechanical strength during the curing and drying stages. Moreover, the calcium aluminates resulted from the decomposition of the hydrates would react with the alumina, increasing the amount of CA_2 and CA_6. On the other hand, the dispersion of calcium aluminate particles in the ACD composition could result in a more uniform microstructure, due to a better dispersed suspension. After the addition of this binder system to the alumina foam, the dispersed CAC would be distributed among the alumina particles. Consequently, denser struts could be generated, increasing the mechanical strength. Additionally, more CA_6 could be formed, reducing the thermal conductivity of the samples. The samples' microstructures after firing at 1600°C for 5h can be observed in the Fig. 6 (a-c). The size of pores, their distribution and morphology can be seen in these figures.

In the Fig. 6, AC sample presented larger pores when compared to the other systems. In agreement with the porosity measurements (Fig. 2), all samples contained pores partially open. Besides the higher amount of closed pores, the composition containing lithium also had cells with smaller

diameters, as observed in the pore size distribution curves in the Fig. 6. On the other hand, AC sample had a wider distribution of pore sizes, with values ranging from few unities of micrometres to values superior than 50 µm. The sample containing dispersed CAC particles presented a narrower distribution of pore sizes, with diameters close to those of the ACA composition. Based on the Fig. 6, half of the pores in the sample AC had sizes equal or below 17 µm. In the same conditions, 50% of the pores in the ACA and ACD samples were below 5 µm and 7.5 µm, respectively.

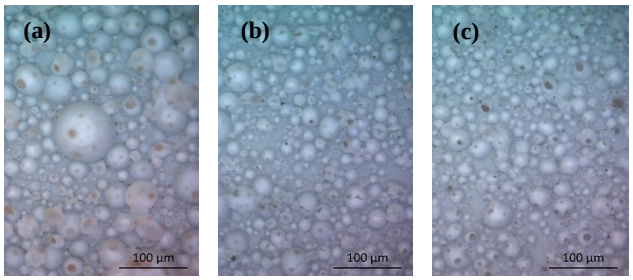

Fig. 6: Microstructure of polished faces of (a) AC, (b) ACA and (c) ACD samples after firing at 1600°C for 5h.

Considering that smaller pores are their higher effectiveness on the thermal insulation at elevated temperatures, these results suggest that ACA and ACD samples would present better thermal insulating properties. For the ACA composition, the faster solidification of the liquid foam avoided the changes in the microstructure caused by drainage, coarsening and coalescence. The same effect on the kinetics of solidification wasn't observed for the ACD samples. Nevertheless, the dispersion of cement particles caused a reduction on the pore size. The hypothesis that the size of a bubble is proportional to the size of the particle adsorbed on its interface emerges from this result. This effect should be further explored as an alternative to stabilise smaller pores in the microstructure of thermal insulating macroporous ceramics.

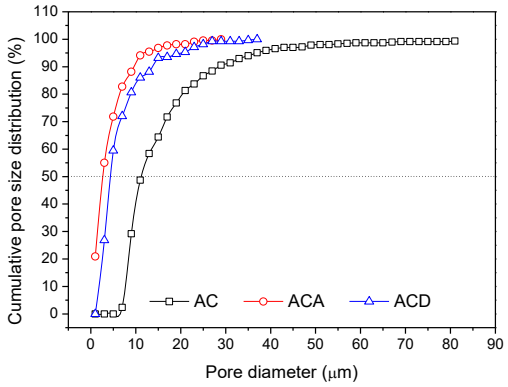

Fig. 7: Cumulative pore size distribution as a function of the diameter of pores measured from polished surfaces of samples fired at 1600°C for 5h.

CONCLUSIONS

The effect of speeding up the hydration or dispersion of calcium aluminate cement on the microstructure of alumina foams for thermal insulation was studied in this work. Besides the distinct kinetics of solidification observed, the results pointed out that denser samples with a higher amount of closed pores were attained when lithium carbonate or dispersed cement particles were used. The cold crushing strength increased when the lithium source was added to the composition and reached the higher values when the cement particles were dispersed. When compared to the composition without lithium source and no dispersed cement particles, the evolution of the mechanical strength verified to systems with lithium source or dispersed CAC particles could be related to the higher amount of hydrates formed, which were better scattered in the microstructure. Additionally, denser struts could be generated when the dispersed cement particles were added. Narrower distributions of pore sizes were attained with the acceleration of the hydration or the dispersion of cement.

These results pointed out that the fast transition of liquid foam to a solid inhibited the transformations of the microstructure caused by drainage, coarsening and coalescence. Additionally, small particles resulted from the deflocculation of cement seems to stabilise smaller pores. Based on these mechanisms, insulating ceramics with higher mechanical strength and closed porosity were generated. Thus, the selection of the binder system was pointed out as an interesting route in order to produce macroporous ceramics with adjusted microstructures.

ACKNOWLEDGEMENTS

The authors are grateful to FIRE and Capes for their support to the present work.

BIBLIOGRAPHY

[1] Vivaldini DO, Mourão AAC, Salvini VR, Pandolfelli VC. Review : Fundamentals and materials for the microstructure design of high performance refractory thermal insulating, Cerâmica. 60 (2014) 297–309..

[2] Ohji T, Fukushima M. Macro-porous ceramics: processing and properties, Int. Mater. Rev. 57 (2012) 115–131.

[3] Studart AR, Gonzenbach UT, Tervoort E, Gauckler LJ, Processing routes to macroporous ceramics: A review, J. Am. Ceram. Soc. 89 (2006) 1771–1789.

[4] Salvini VR, Lasso PRO, Luz AP, Pandolfelli VC. Nontoxic Processing of reliable macro-porous ceramics, Int. J. Appl. Ceram. Technol. 13 (2016) 522–531.

[5] Rodger SA, Double DD. The chemistry of hydration of high alumina cement in the presence of accelerating and retarding admixtures, Cem. Concr. Res. 14 (1984) 73–82.

[6] ASTM International, Standard test methods for cold crushing strength and modulus of rupture of refractories (C133-97), (2003) 1–6.

[7] Scheffler M, Colombo P. Cellular Ceramics, Wiley-VCH Verlag GmbH & Co. KGaA, Weinheim, FRG, 2005.

[8] Auvray JM, Gault C, Huger M. Evolution of elastic properties and microstructural changes versus temperature in bonding phases of alumina and alumina–magnesia refractory castables, J. Eur. Ceram. Soc. 27 (2007) 3489–3496.

MAILING ADDRESS

tiagosjunior@ppgcem.ufscar.br